ACS APPLIED NANO MATERIALS

www.acsanm.org Article

Structure–Property–Performance Relationships of Dielectric Cu_2O Nanoparticles for Mie Resonance-Enhanced Dye Sensitization

Ravi Teja Addanki Tirumala, Sundaram Bhardwaj Ramakrishnan, Farshid Mohammadparast, Nishan Khatri, Swetha Mahalakshmi Arumugam, Susheng Tan, A. Kaan Kalkan, and Marimuthu Andiappan*

Cite This: *ACS Appl. Nano Mater.* 2022, 5, 6699–6707 Read Online

ACCESS | Metrics & More | Article Recommendations | Supporting Information

ABSTRACT: A dye-sensitized photocatalytic (DSP) approach is considered as one of the promising approaches for developing visible light- and near-infrared light-responsive photocatalysts. DSP systems are still affected by significant drawbacks, such as low light absorption efficiency. Recently, it has been demonstrated that the plasmonic metal nanostructures can be used to enhance the light absorption efficiency and the overall dye-sensitization rate of DSP systems through the plasmonic Mie resonance-enhanced dye-sensitization approach. In this contribution, we report an alternate and novel approach, dielectric Mie resonance-enhanced dye sensitization. Specifically, we demonstrate that the dielectric Mie resonances in cuprous oxide (Cu_2O) spherical and cubical nanostructures can be used to enhance the dye-sensitization rate of methylene blue dye. The Cu_2O nanostructures exhibiting dielectric Mie resonances exhibit up to 1 order of magnitude higher dye-sensitization rate as compared to Cu_2O nanostructures not exhibiting dielectric Mie resonances. Our model system developed from finite-difference time-domain simulation predicts a volcano-type relationship between the dye-sensitization rate and the size of Cu_2O nanostructures. The predicted structure–property–performance relationship is experimentally verified, and the optimal size ranges of Cu_2O nanospheres and nanocubes are identified. Although we demonstrate the dielectric Mie resonance-enhanced dye-sensitization approach using Cu_2O nanostructures, the proposed approach can be used to design a wide range of DSP systems, including CeO_2, α-Fe_2O_3, and TiO_2 nanostructure-based DSP systems.

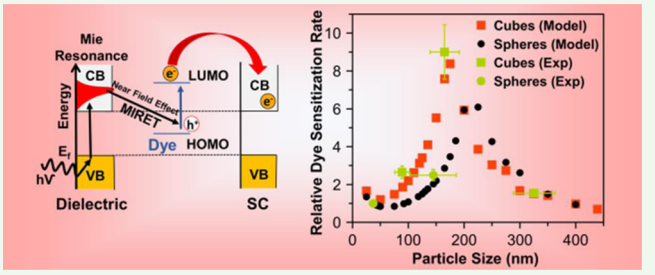

KEYWORDS: *dye sensitization, mie resonance, dielectric resonance, metal oxide, semiconductor*

1. INTRODUCTION

Dye-sensitized photocatalytic (DSP) systems have emerged as a promising approach for a number of applications, including renewable hydrogen (H_2) production via photocatalytic water splitting, photocatalytic conversion of carbon dioxide (CO_2) into value-added products, and pollution mitigation. In a typical DSP system, a dye molecule is used as a photosensitizer that is adsorbed on a semiconductor nanostructure. As shown in Figure 1a, in the DSP system, the dye molecules absorb incident light and inject the excited electrons into the conduction band (CB) of the semiconductor. These excited electrons can be used to drive reduction reactions, such as the reduction of water for H_2 production. The regeneration of the dye molecule for cyclic utilization can be accomplished using the electron donor. In the last 2 decades, significant progress has been made in the field, and studies have shown that by appropriately selecting and matching the energy levels of dye molecules and semiconductors, DSP systems can be designed to cover the visible region and even the near-infrared region of the solar spectrum. Despite these great successes achieved in the field, DSP systems are still affected by significant drawbacks, such as low light absorption efficiency.[1−5]

Recently, it has been demonstrated that plasmonic Mie resonances of metal nanostructures, such as silver (Ag) and gold (Au) can be used to enhance the light absorption efficiency of dye molecules in the DSP and photovoltaic systems.[6−17] The plasmonic metal nanostructures (PMNs) under Mie resonance conditions can exhibit very high absorption cross-sectional values that are up to 5 orders of magnitude higher than those of dye molecules.[18−20] Therefore, a PMN (e.g., Ag and Au) can harvest a large fraction of the incident light and transfer the energy into the nearby dye molecules and enhance their light absorption efficiency via a

Received: February 17, 2022
Accepted: April 29, 2022
Published: May 11, 2022

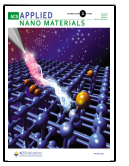

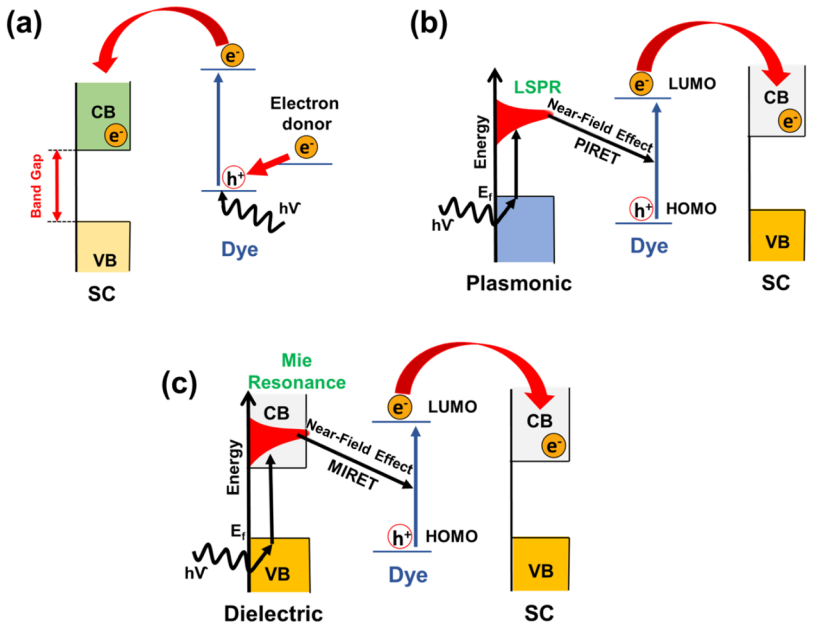

Figure 1. Schematic diagram of (a) dye sensitization and electron transfer into the CB of the semiconductor (SC), (b) localized surface plasmon resonance (LSPR)-enhanced dye sensitization, and (c) dielectric Mie resonance-enhanced dye sensitization.

number of pathways, including the nanoantenna effect and plasmon-induced resonance energy transfer (Figure 1b).[21−23] These plasmonic Mie resonance-mediated effects are utilized to enhance the rate of dye sensitization in DSP systems. However, these PMN-based DSP systems also possess inherent challenges, such as compatibility issues with conventional semiconductor manufacturing, high material costs, and issues of commercialization with increasing complexity due to the need for both metals and semiconductors.

Herein, we propose a solution to the aforementioned issues through an alternate approach, dielectric Mie resonance-enhanced dye sensitization, as shown schematically in Figure 1c. The Mie resonances can occur in plasmonic materials that exhibit negative permittivity ($\varepsilon < 0$) as well as dielectric ($\varepsilon > 0$) materials with moderate (2.5−3.5) and high refractive index values (>3.5).[24−32] The condition for the dielectric Mie resonance to occur in the medium- and high-refractive-index spherical particles is $d = 2R \sim \lambda/n$, where R is the radius of the particle, λ is the wavelength of light, and n is the refractive index of the material.[27] The dielectric Mie resonance-enhanced dye sensitization proposed in Figure 1c is, therefore, most suitable for DSP systems built on metal oxide semiconductors with moderate and high refractive index values. Such metal oxide semiconductors include cerium(IV) oxide (CeO_2), cuprous oxide (Cu_2O), hematite iron oxide (α-Fe_2O_3), and titanium dioxide (TiO_2).

Similar to the plasmonic Mie resonances of PMNs, the dielectric Mie resonances of nanostructures of medium- and high-refractive-index metal oxide semiconductors can transfer the photonic energy into the adsorbed dye molecules via pathways such as the nanoantenna effect, resonance energy transfer, and Mie resonance-mediated intense scattering effect. These dielectric Mie-resonance effects are expected to enhance the light absorption efficiency of the dye molecules in the DSP systems (Figure 1c). One major difference is that, unlike the plasmonic Mie resonance-based system (Figure 1b), in a dielectric Mie resonance-based system (Figure 1c), there is no need for a separate light-enhancing material. Being a major advantage, this system solely requires a dielectric semiconductor nanostructure and a dye. Specifically, the dielectric semiconductor nanostructure can play the role of a Mie resonator for enhancing the light absorption efficiency of the dye molecule as well as a source for harvesting excited electrons from the dye molecules and facilitating the reduction reaction (Figure 1c).

In this contribution, we demonstrate the dielectric Mie resonance-enhanced dye-sensitization approach using methylene blue (MB) dye sensitization on Cu_2O nanostructures as an example. We have developed the structure−property−performance relationships of Cu_2O nanostructures for MB dye sensitization. Specifically, different sizes of Cu_2O nanospheres and nanocubes are synthesized, and the structure of these Cu_2O nanostructures is characterized using transmission electron microscopy (TEM) and scanning electron microscopy (SEM). The size-dependent optical properties of the Cu_2O nanospheres and nanocubes are predicted using finite-difference time-domain (FDTD) simulations. Based on these FDTD simulation results, we predict a volcano-type relationship between the size of Cu_2O nanostructures and the enhancement of the dye-sensitization rate by the respective nanostructures. The predicted structure−property−performance relationships of Cu_2O nanospheres and nanocubes are experimentally verified by measuring the rate of MB dye sensitization followed by dye degradation (DSD).

2. EXPERIMENTAL SECTION

The procedures followed for FDTD simulations, syntheses (Scheme 1a−c) and characterizations of Cu_2O nanospheres and nanocubes,[24,33,34] and MB dye-sensitization and -degradation experiments are detailed in the Supporting Information. Briefly, Cu_2O nanospheres with average diameters of 37 and 145 nm and Cu_2O nanocubes with average edge lengths of 92, 165, and 325 nm were synthesized using the synthesis protocols reported in our previous contributions.[24,33,34] The sizes and Cu_2O phases of the nanostructures were confirmed using TEM and SEM and X-ray diffraction patterns, respectively (Figure S1a,b in Supporting Information). The performance of the Cu_2O nanostructures toward MB dye sensitization was evaluated

https://doi.org/10.1021/acsanm.2c00730
ACS Appl. Nano Mater. 2022, 5, 6699−6707

Scheme 1. Schematic Representation of Nanoparticle's Synthesis Using a (a) Microemulsion Technique for Obtaining Quasi-Spherical Cu_2O Nanoparticles of 37 nm Diameter, (b) Chemical Reduction Method to Obtain Cu_2O Nanocubes, and (c) Chemical Reduction Method to Obtain Quasi-Spherical Cu_2O Nanoparticles of 145 nm Diameter

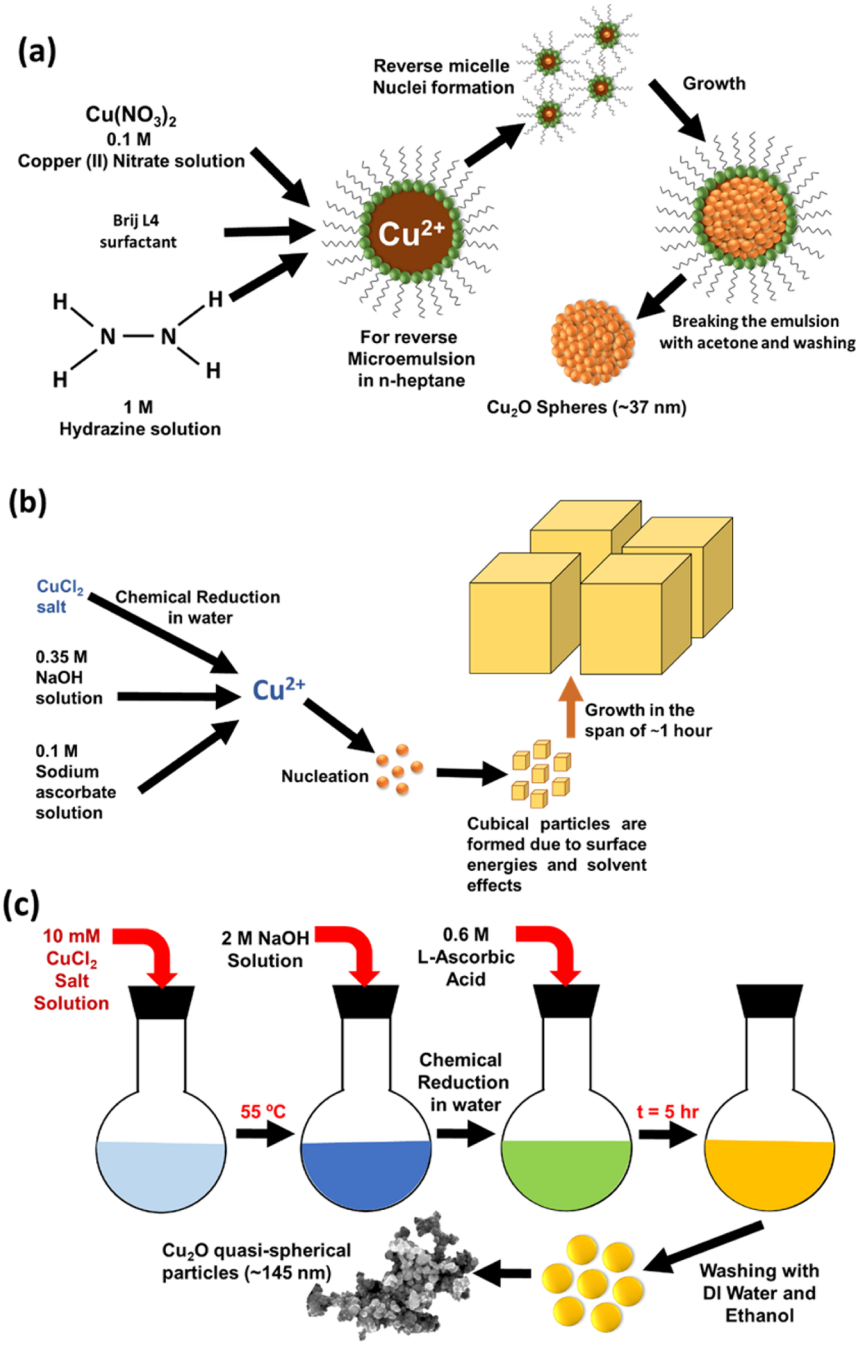

through the measurement of the rate of MB degradation that occurs in the MB dye-sensitization region. The MB degradation was carried out in the solution phase using dimethylformamide (DMF) as a solvent. To quantify the extent of MB degradation, the concentration of MB in the reaction mixture was quantified as a function of irradiation time. The MB absorption value at its peak absorption wavelength (i.e., 665 nm) in the ultraviolet−visible (UV−vis) absorption spectrum was used to quantify the concentration of MB.

3. RESULTS AND DISCUSSION

Figure 2a−d shows the representative TEM and SEM images of quasi-spherical Cu_2O nanoparticles with an average diameter of 37 and 145 nm and Cu_2O nanocubes with an average edge length of 165 and 325 nm, respectively. Figure 2e,f shows the experimentally measured UV−vis−near-IR extinction spectra of these Cu_2O nanostructures. The representative SEM image and UV−vis−near-IR extinction spectra of Cu_2O nanocubes of 92 nm average edge length are also provided in Figure S1d,e in Supporting Information. The extinction spectra shown in Figure 2e,f are consistent with the extinction features predicted from the FDTD simulations (Figure S2a−d in Supporting Information). Specifically, as seen from Figure 2e, Cu_2O nanospheres of 37 nm average diameter exhibit extinction features similar to the bulk Cu_2O, which is a semiconductor with a band gap of 2.1 eV.[24] For

https://doi.org/10.1021/acsanm.2c00730
ACS Appl. Nano Mater. 2022, 5, 6699−6707

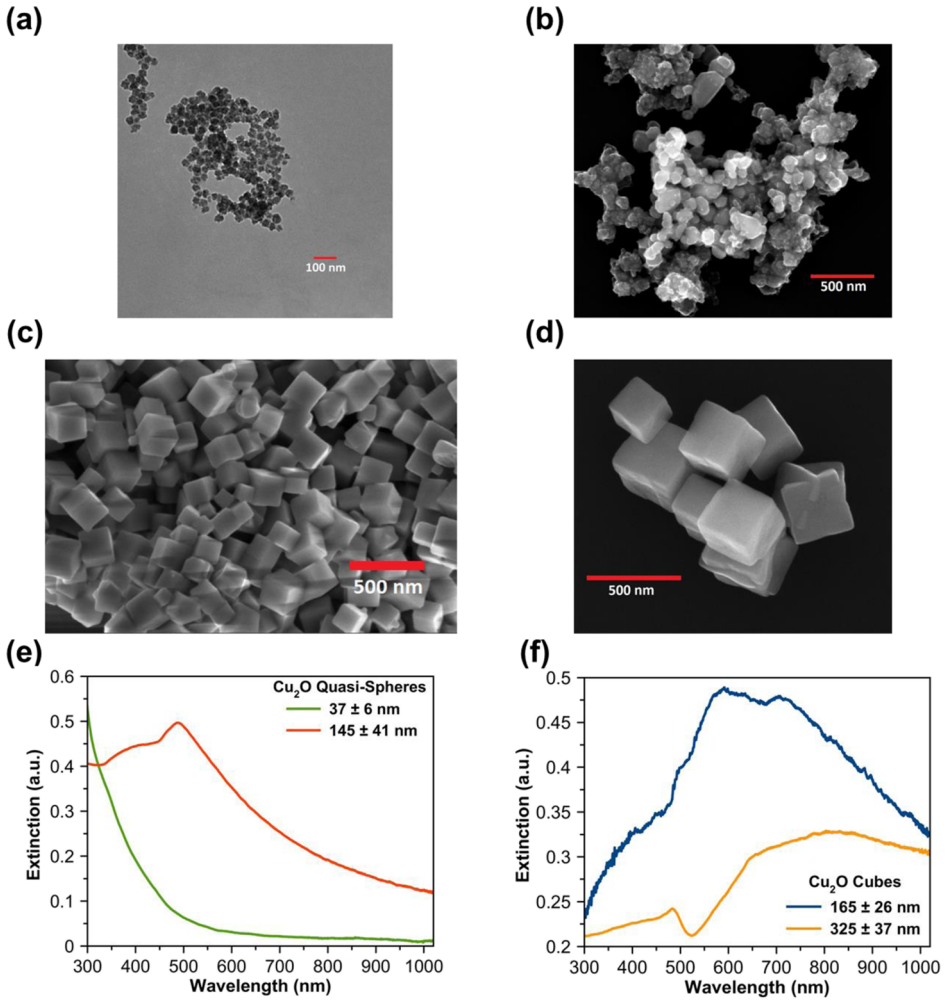

Figure 2. (a–d) Representative TEM and SEM images of (a) quasi-spherical Cu_2O nanoparticles of 37 ± 6 nm diameter, (b) quasi-spherical Cu_2O nanoparticles of 145 ± 41 nm diameter, (c) Cu_2O nanocubes of 165 ± 26 nm edge length, and (d) Cu_2O nanocubes of 325 ± 37 nm edge length. UV–vis–near-IR extinction spectra of (e) quasi-spherical Cu_2O nanoparticles of 37 ± 6 and 145 ± 41 nm diameters, and (f) Cu_2O nanocubes of 165 ± 26 and 325 ± 37 nm edge lengths, dispersed in DMF.

these 37 nm Cu_2O nanospheres, the dielectric Mie resonances are absent in the UV–vis–near-IR regions. In contrast, Cu_2O nanospheres and nanocubes of sizes larger than 90 nm exhibit strong dielectric Mie resonances in the UV–vis–near-IR regions, as shown in Figure 2e,f (also see Figures S1e and S2a–d in Supporting Information). The lowest Mie resonance peak in the UV–vis–near IR extinction spectrum corresponds to the combination of the electric dipole and magnetic dipole (Figure S2e in Supporting Information).[24] Similarly, the second-lowest energy peak and higher-order peaks correspond to the combination of the electric quadrupole and magnetic quadrupole and the combination of higher-order electric and magnetic modes, respectively (Figure S2f in Supporting Information).[24]

To evaluate the performance of the Cu_2O nanostructures toward the MB DSD, we have selected red LEDs as the illumination source. The intensity of the light, when measured at the surface of the photoreactor, was 7.49 mW/cm^2, and it was kept constant for all dye-sensitization experiments reported in this contribution. In Figure 3a, we show the spectrum of red LEDs and UV–vis absorption spectrum of MB dye. As seen from Figure 3a, there is a significant overlap between the spectrum of red LEDs and the absorption spectrum of MB in the 590–670 nm region. It has been previously shown that in this region (590–670 nm), MB molecules can undergo dye sensitization and inject the excited electrons into the CB of the semiconductor (Figure 3b).[35,36] In the presence of dissolved oxygen (O_2), these electrons can form superoxide (O_2^-), which can attack and cause the degradation of excited MB molecules (Figures 3b and S5).[35,36] We also confirmed the role of superoxide using the experiments in the presence of a superoxide quencher in the system. In our study, the quenching experiments were performed in the presence of benzoquinone, which is a well-known superoxide quencher. No significant MB degradation was observed in these experiments (Figure S6). These results confirm that the DSD of MB in our system occurs via a superoxide-mediated pathway (e.g., Figure 3b). Also, since the band gap of Cu_2O is 2.1 eV (~590 nm),[24,37] the rate of MB degradation via direct photocatalysis by Cu_2O nanostructures is expected to be minimal in this MB dye-sensitization region (590–670 nm) investigated in this study.

To illustrate the role of dielectric Mie resonances in the MB dye sensitization, we carried out the experiments to quantify the rate of MB DSD using quasi-spherical Cu_2O nanoparticles with an average diameter of 145 nm and Cu_2O nanocubes with

https://doi.org/10.1021/acsanm.2c00730
ACS Appl. Nano Mater. 2022, 5, 6699–6707

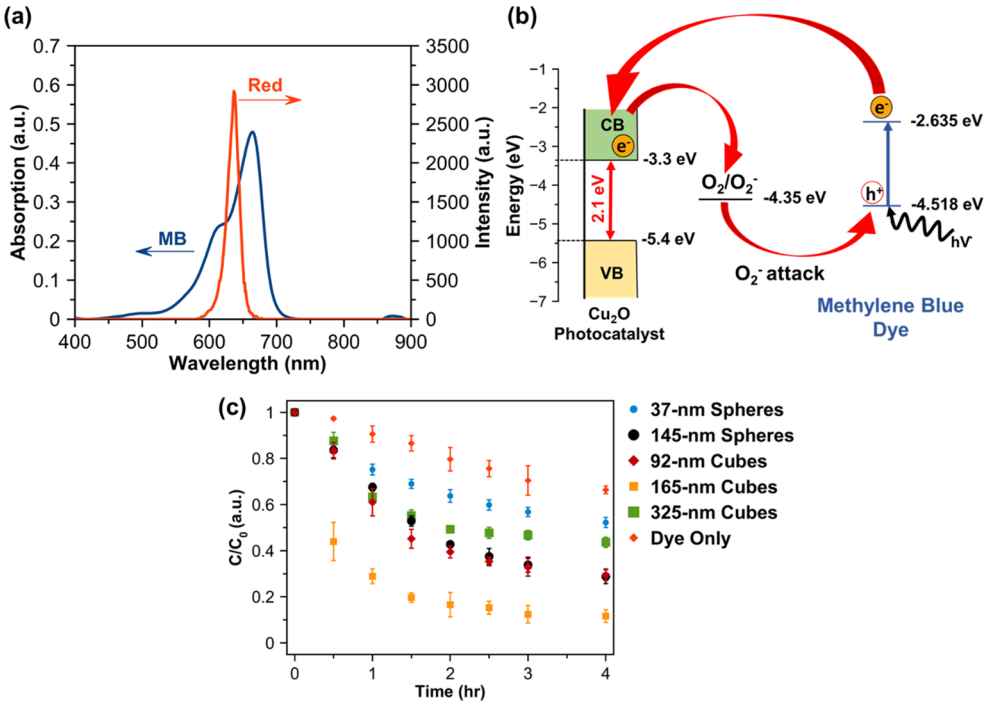

Figure 3. (a) Absorption spectrum of MB (left ordinate) and the spectrum of the red LED light source used for MB dye sensitization (right ordinate). (b) Schematic diagram illustrating the MB DSD via superoxide (O_2^-) intermediate species.[38,39] (c) Plot of C/C_0 vs irradiation time for MB DSD in DMF using quasi-spherical Cu_2O nanoparticles of 37 ± 6 nm diameter (blue circles), quasi-spherical Cu_2O nanoparticles of 145 ± 41 nm diameter (black circles), Cu_2O nanocubes of 92 ± 13 nm edge length (maroon diamonds), Cu_2O nanocubes of 165 ± 26 nm edge length (orange squares), Cu_2O nanocubes of 325 ± 37 nm edge length (green squares), and under blank conditions in the absence of the photocatalyst (red triangles).

an average edge length of 92, 165, and 325 nm. These Cu_2O nanostructures exhibit dielectric Mie resonances in the MB dye-sensitization region (590−670 nm), as seen from Figure 2e,f. We also carried out the same experiments using quasi-spherical Cu_2O nanoparticles with an average diameter of 37 nm, in which the dielectric Mie resonances are absent in the MB dye-sensitization region (Figure 2e). In these dye-sensitization experiments performed with different sizes of Cu_2O nanospheres and nanocubes, the weight load of the Cu_2O nanostructures in the reaction mixture was kept constant. Before exposing the reaction mixture to the red-light illumination, the MB dye molecules were stirred with Cu_2O nanostructures dispersed in DMF for 3 h to reach the adsorption equilibrium. Also, the reaction mixture was sparged with air for 30 min to start all experiments with the same level of dissolved oxygen. Figure 3c shows the extent of MB degradation (C/C_0) under the red-light illumination (590−670 nm) conditions in the presence of different sizes of Cu_2O nanospheres and nanocubes and also in the absence of Cu_2O nanostructures.

As seen from Figure 3c, the slowest rate of MB degradation is observed for the dye-only conditions carried out in the absence of Cu_2O nanostructures. For the experiments performed in the presence of different sizes of Cu_2O nanospheres and nanocubes, the Cu_2O nanostructures with dielectric Mie resonances exhibit a higher rate of MB degradation than the 37 nm quasi-spherical Cu_2O nanoparticles that exhibit no Mie resonance in the dye-sensitization region. Specifically, the increasing rate of MB degradation is observed in the following order: 165 nm Cu_2O nanocubes >92 nm Cu_2O nanocubes >145 nm quasi-spherical Cu_2O nanoparticles >325 nm Cu_2O nanocubes >37 nm quasi-spherical Cu_2O nanoparticles (also see Table S1 in Supporting Information). To investigate the possible role of the light-induced heating effect on MB degradation, we measured the light-induced increase in the temperature of the reaction mixture. We found that the temperature of the reaction mixture increased from ∼20 to ∼30 °C under MB dye-sensitization conditions (Figure S3a−e in Supporting Information). This increase in the temperature was uniform for all experiments performed in the presence of different sizes of Cu_2O nanospheres and nanocubes as well as for the experiments performed in the absence of Cu_2O nanostructures (Figure S3a−e in Supporting Information). We also performed heating experiments at an elevated temperature of 60 °C. No significant degradation was observed in these heating experiments performed under dark conditions in the absence of red-light irradiation (Figure S3f in Supporting Information). These results confirm that the difference in the rate of MB degradation observed in the presence of Cu_2O nanospheres and nanocubes of different sizes is not due to the light-induced heating effect. Therefore, we attribute the higher rate of MB degradation observed with the Cu_2O nanostructures with dielectric Mie resonances (e.g., 165 nm Cu_2O nanocubes) in Figure 3c to the dielectric Mie resonance-enhanced MB dye sensitization.

For the dye-only conditions, in the absence of Cu_2O nanostructures, the MB degradation can occur via the absorption of the incident photons by the dye molecules, followed by the photoexcited electron transfer from the excited MB molecules into the dissolved oxygen to form superoxide radicals (O_2^-). The superoxide radicals can then attack and degrade the excited MB molecules (Figure S4a in Supporting Information).[35] The Cu_2O nanostructures can enhance the

https://doi.org/10.1021/acsanm.2c00730
ACS Appl. Nano Mater. 2022, 5, 6699−6707

light absorption efficiency of the dye molecules via a number of pathways, including the electromagnetic near-field or nano-antenna effect and Mie resonance-induced resonance energy transfer (MIRET). The Cu_2O nanostructures can also facilitate and enhance the electron transfer between adsorbed MB and O_2 molecules and the subsequent degradation of the excited MB molecules. In this contribution, to develop the structure−property−performance relationships of Cu_2O nanostructures for MB DSD, we propose the following simple approximation shown in eq 1 (see the Supporting Information for more details). This equation relates the rate of MB DSD that occurs via the dye-sensitization pathway in the presence of Cu_2O nanostructures and the optical and geometrical properties of the respective Cu_2O nanostructures.

$$r \propto \int I_0(\lambda)\mathrm{Abs}_{\mathrm{MB}}(\lambda)E_{\mathrm{Cu_2O}}(\lambda)\mathrm{d}\lambda \times \frac{S}{V} \quad (1)$$

where r is the rate of DSD per unit mass of the Cu_2O nanostructures, $\mathrm{Ext}_{\mathrm{Cu_2O}}$ is the volume-normalized extinction cross section of the Cu_2O nanostructure, $\mathrm{Abs}_{\mathrm{MB}}$ is the absorbance of MB, I_0 is the intensity of the incident light, λ is the wavelength of the incident light, and S and V are the surface area and volume of the Cu_2O nanostructure, respectively. Equation 1 predicts that the optimal overlap between the extinction spectrum of Cu_2O nanostructures, the absorption spectrum of dye molecules, and the incident light spectrum will result in the optimal rate of dye sensitization.

To predict the structure−property−performance relationships of Cu_2O nanostructures using eq 1, we performed FDTD simulations of Cu_2O nanospheres and nanocubes of different sizes (25−400 nm) and simulated the extinction cross section of the respective nanostructures as a function of incident light wavelength. The representative FDTD-simulated extinction spectra of these Cu_2O nanocubes are provided in Figure 4a (also see Figure S4b−e in Supporting Information). Based on eq 1, in Figure 4a, the extinction cross-sectional values are normalized to the fourth power of the edge length. These FDTD-simulated values are used in eq 1 to predict the performance of Cu_2O nanospheres and nanocubes of different sizes in the range of 25−400 nm. Figure 4b shows the rate of MB degradation that can occur in the dye-sensitization region (590−670 nm) in the presence of these Cu_2O nanostructures. In Figure 4b, the rate values in the y-axis are normalized with respect to the Cu_2O nanosphere of 37 nm diameter. As seen from Figure 4b, our model that is based on eq 1 and FDTD-simulated extinction cross-sectional values predicts a volcano-type relationship between the rate of DSD and the size of Cu_2O nanostructures. The volcano-type relation between the DSD rate and particle size in Figure 4b originates from the spectral shift of dielectric Mie modes (resonances) with size. From the kinetic data collected from the experiments performed with quasi-spherical Cu_2O nanoparticles of 37 and 145 nm average diameters and Cu_2O nanocubes of 92, 165, and 325 nm edge lengths (Figure 3c), we calculated the relative rate of DSD for these Cu_2O nanostructures (see Figure S4v−z and Table S1 in Supporting Information for more details). As seen from Figure 4b, the experimentally measured values are in well agreement with the predicted values. The optimum sizes of Cu_2O nanospheres and nanocubes in the volcano plot shown in Figure 4b are in the range of 165−200 nm for the MB molecules-based DSP system. The main reason for these Cu_2O nanostructures to appear in the optimum range

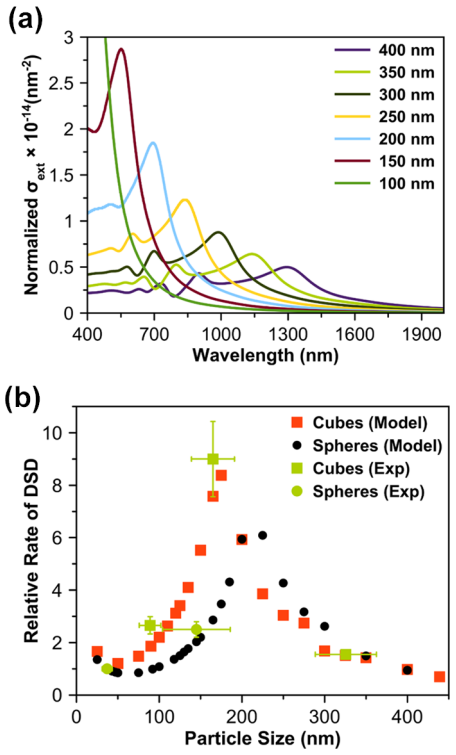

Figure 4. (a) FDTD-simulated normalized-extinction (normalized-σ_{Ext}) cross section of Cu_2O nanocubes of different edge lengths in the range of 100−400 nm as a function of incident light wavelength. Normalized-σ_{Ext} = ratio of extinction cross section (σ_{Ext}) of the nanocube to the fourth power of its edge length (A^4). (b) Volcano plot showing the predicted and experimentally measured relative rates of MB DSD as a function of size of Cu_2O nanospheres and nanocubes. Black circles and red squares represent predicted relative rates for Cu_2O nanospheres and nanocubes, respectively. Green circles and green squares represent experimentally measured relative rates on quasi-spherical Cu_2O nanoparticles of 37 ± 6 nm diameter, quasi-spherical Cu_2O nanoparticles of 145 ± 41 nm diameter, Cu_2O nanocubes of 92 ± 13 nm edge length, Cu_2O nanocubes of 165 ± 26 nm edge length, and Cu_2O nanocubes of 325 ± 37 nm edge length, respectively. The rate of MB DSD on quasi-spherical Cu_2O nanoparticles of 37 ± 6 nm diameter is used as a reference.

is their high extinction cross-sectional values in the MB dye-sensitization region (i.e., 590−670 nm), as seen from Figure 4a. Moreover, the dielectric Mie resonance-enhanced dye sensitization causes the 165 nm nanocubes to exhibit approximately 1 order of magnitude (∼9 times) higher dye-sensitization rate as compared to 37 nm nanospheres, in which the Mie resonance is absent (see Figure 4b and Table S1 in Supporting Information).

The structure−property−performance relationships developed in this contribution can be used for designing a wide range of other DSP systems. For example, when the Cu_2O nanostructures are used for DSP system consisting of a dye that absorbs in the shorter wavelength region (e.g., 460−500 nm), our model shown in eq 1 predicts that optimum sizes of Cu_2O nanostructures move toward smaller sizes (e.g., 120−150 nm Cu_2O nanocubes in Figure 4a). Similarly, for dyes that can absorb in the near-IR wavelength region (e.g., 800−900 nm), the optimum sizes are predicted to move toward larger sizes (e.g., 240−270 nm Cu_2O nanocubes in Figure 4a). The approach demonstrated in this study can also be used to design DSP systems that can involve a wide range of combinations of

https://doi.org/10.1021/acsanm.2c00730
ACS Appl. Nano Mater. 2022, 5, 6699−6707

medium- and high-refractive-index semiconductors and dye molecules. Our FDTD simulation results shown in Figure S4f–u in the Supporting Information predict that such combinations can include semiconductors such as CeO_2, CuO, α-Fe_2O_3, and TiO_2 and appropriate dye molecules that can absorb anywhere in the visible and near-IR wavelength regions. The energy levels of these dye molecules need to be in alignment with the conduction bandedge of the semiconductors so that the excited electrons can be transferred from the dye molecules into the semiconductor.

To investigate the stability of Cu_2O nanoparticles under the investigated DSD conditions, Raman spectroscopy of the quasi-spherical Cu_2O nanoparticles of 145 ± 41 nm diameter was performed with a WITec alpha300 R confocal Raman microscope, equipped with a 532 nm laser. Ensemble-averaged acquisitions were sampled from Cu_2O aggregates after aliquots of 0.1 mL were directly spotted from colloidal suspensions on microscope slides and left to dry. For single-particle acquisitions, the colloids were diluted 100× in ethanol before spotting and drying. The single particles were located from their strong Mie scattering images (diffraction-limited). Spectra of aggregates were collected using a 20× objective lens of 0.40 numerical aperture (NA). Spectra of single nanospheres were acquired using a 100× objective lens of 0.90 NA. We employed a 600 lines/mm grating and 100 μm confocal aperture (fiber diameter). The laser spot diameters were adjusted to 25 and 5 μm, respectively. The signal was integrated for 100 s. The laser power was optimized (maximized) to the onset of spectral shifting, caused by laser heating.

Representative Raman spectra of ensembles (aggregates) and single particles are shown in Figure 5a,b, respectively, for the following three cases: the as-prepared fresh Cu_2O nanoparticles; Cu_2O nanoparticles after equilibrating with MB and before exposing to light illumination (t = 0 h); and Cu_2O nanoparticles exposed to 4 h of light illumination under DSD conditions (t = 4 h). In Figure 5a,b, the strongest Raman peak at 215 cm^{-1} is a second-order overtone $2\Gamma_{12}^{-}$, which is characteristic of crystalline Cu_2O.[24] The second strongest peak at 630 cm^{-1} is assigned to the infrared-allowed Γ_{15}^{-} (TO) mode in Cu_2O crystals.[24] The third strongest peak at 415 cm^{-1} is attributed to the overtone of four phonons, $3\Gamma_{12}^{-} + \Gamma_{25}^{-}$, in crystalline Cu_2O.[24] On the other hand, the strongest characteristic peaks of CuO, being at 298, 330, and 602 cm^{-1}, are not detected.[24] Therefore, all spectra are characteristic of Cu_2O, and the CuO phase is not detectable. These results confirm that Cu_2O nanoparticles are stable and do not undergo oxidation under the DSD conditions investigated in this study.

4. CONCLUSIONS

In conclusion, we have demonstrated that the rate of dye sensitization can be enhanced in the presence of semiconductor nanostructures with dielectric Mie resonances. Using FDTD simulation results, we have developed the structure–property–performance relationship for the dielectric Mie resonance-enhanced dye sensitization. The predicted volcano-type relationship between the rate of MB dye sensitization and the size of Cu_2O nanostructures is experimentally verified using the rate measurements of MB DSD in the presence of Cu_2O nanospheres and nanocubes of different sizes. The flexibility of tuning the dielectric Mie resonance peaks across the visible and near-IR regions by controlling the size of the dielectric nanostructures marks their applicability to a wide range of DSP systems. Specifically, the findings of this contribution open a novel approach to design efficient DSP systems that can involve semiconductors such as CeO_2, CuO, Cu_2O, α-Fe_2O_3, and TiO_2 and a wide range of visible- and near-IR-responsive dye molecules.

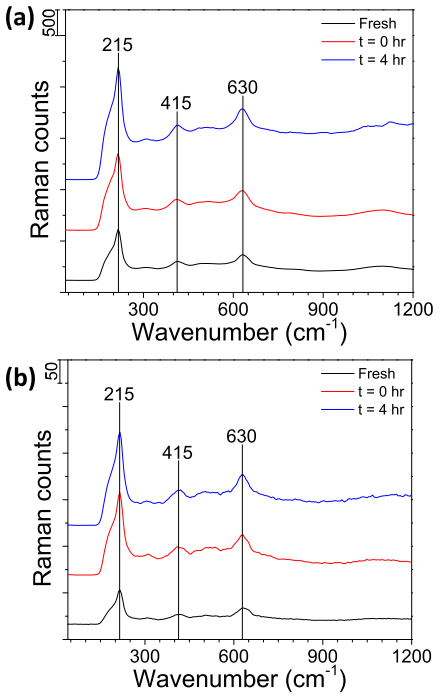

Figure 5. Representative Raman spectra of quasi-spherical Cu_2O nanoparticles of 145 ± 41 nm diameter samples for the three cases: fresh; t = 0; and t = 4 h. The spectra shown in (a,b) are measured from ensembles (aggregates) and single particles, respectively. Fresh samples are the as-prepared Cu_2O samples. The T = 0 h sample represents Cu_2O particles after equilibrating with MB and before exposing them to light illumination. The T = 4 h sample represents after 4 h of light illumination under DSD conditions.

■ ASSOCIATED CONTENT

Supporting Information

The Supporting Information is available free of charge at https://pubs.acs.org/doi/10.1021/acsanm.2c00730.

Syntheses and characterizations of Cu_2O nanostructures; detailed experimental methods of DSD experiments; computational details for FDTD simulations; X-ray diffraction patterns of Cu_2O nanospheres and nanocubes; Luzchem photoreactor experimental setup with red light illumination used for dye-sensitization studies; TEM image of large Cu_2O nanocubes; UV extinction spectrum of Cu_2O nanocubes; FDTD-simulated normalized-extinction cross section of Cu_2O nanospheres of different edge lengths in the ranges of 25–200 and 250–400 nm; FDTD-simulated normalized-extinction cross section of Cu_2O nanocubes of different edge lengths in the ranges of 25–200 and 250–400 nm; simulated spatial distribution enhancements of electric field intensity in the XY plane at different wavelengths (598 and 415 nm) across the Mie resonance peak wavelength for Cu_2O nanocubes; simulated spatial distribution enhancement of magnetic field intensity in the YZ plane at different wavelengths across the Mie resonance

https://doi.org/10.1021/acsanm.2c00730
ACS Appl. Nano Mater. 2022, 5, 6699–6707

peak wavelengths (598 and 415 nm) for Cu_2O nanocubes; temperature profiles measured as a function of irradiation time for MB DSD in DMF using quasi-spherical Cu_2O nanoparticles with diameters of 37 ± 6 and 145 ± 41 nm; temperature profiles measured as a function of irradiation time for MB DSD in DMF using Cu_2O nanocubes with edge lengths of 165 ± 26 and 325 ± 37 nm; temperature profiles measured as a function of irradiation time for MB DSD in DMF under blank conditions in the absence of a photocatalyst; plot of C/C_0 of MB versus reaction time measured during heating experiments at 60 °C in the presence of large Cu_2O cubes; schematic diagram of the dye-only DSD pathway; FDTD-simulated normalized-extinction cross sections of Cu_2O nanocubes and nanospheres, CeO_2 nanospheres and nanocubes, CuO nanospheres and nanocubes, α-Fe_2O_3 nanospheres and nanocubes, and TiO_2 nanospheres and nanocubes; plots of empirical fit with second order versus irradiation time for MB DSD in DMF using quasi-spherical Cu_2O nanoparticles with diameters of 37 ± 6 and 145 ± 41 nm; plots of empirical fit with second order versus irradiation time for MB DSD in DMF using Cu_2O nanocubes with edge lengths of 165 ± 26, 325 ±37, and 92 ± 13 nm; schematic diagram of the MB DSD via superoxide intermediate species; fitted second-order rate constant values using Cu_2O nanospheres and nanocubes; and real and imaginary parts of refractive index values of Cu_2O used in the simulations(PDF)

AUTHOR INFORMATION

Corresponding Author

Marimuthu Andiappan − *School of Chemical Engineering, Oklahoma State University, Stillwater, Oklahoma 74078, United States;* orcid.org/0000-0002-4211-030X; Email: mari.andiappan@okstate.edu

Authors

Ravi Teja Addanki Tirumala − *School of Chemical Engineering, Oklahoma State University, Stillwater, Oklahoma 74078, United States*

Sundaram Bhardwaj Ramakrishnan − *School of Chemical Engineering, Oklahoma State University, Stillwater, Oklahoma 74078, United States*

Farshid Mohammadparast − *School of Chemical Engineering, Oklahoma State University, Stillwater, Oklahoma 74078, United States*

Nishan Khatri − *School of Mechanical and Aerospace Engineering, Oklahoma State University, Stillwater, Oklahoma 74078, United States*

Swetha Mahalakshmi Arumugam − *Department of Chemistry, PSG College of Arts & Science, Coimbatore 641014, India*

Susheng Tan − *Department of Electrical and Computer Engineering and Petersen Institute of Nano Science and Engineering, University of Pittsburgh, Pittsburgh, Pennsylvania 15261, United States;* orcid.org/0000-0002-6162-7443

A. Kaan Kalkan − *School of Mechanical and Aerospace Engineering, Oklahoma State University, Stillwater, Oklahoma 74078, United States;* orcid.org/0000-0001-5878-3413

Complete contact information is available at: https://pubs.acs.org/10.1021/acsanm.2c00730

Notes

The authors declare no competing financial interest.

ACKNOWLEDGMENTS

We gratefully acknowledge Dr. Andiappan's awarded funding from the National Science Foundation CBET Catalysis Program under grant no. NSF CBET-2102238. We also acknowledge funding from the Oklahoma Center for the Advancement of Science and Technology under the project number HR18-093.

REFERENCES

(1) Zhang, X.; Peng, T.; Song, S. Recent Advances in Dye-Sensitized Semiconductor Systems for Photocatalytic Hydrogen Production. *J. Mater. Chem. A* **2016**, *4*, 2365−2402.

(2) Watanabe, M. Dye-Sensitized Photocatalyst for Effective Water Splitting Catalyst. *Sci. Technol. Adv. Mater.* **2017**, *18*, 705−723.

(3) Huang, J. F.; Lei, Y.; Luo, T.; Liu, J. M. Photocatalytic H2 Production from Water by Metal-Free Dye-Sensitized TiO2 Semiconductors: The Role and Development Process of Organic Sensitizers. *ChemSusChem* **2020**, *13*, 5863−5895.

(4) Reginato, G.; Zani, L.; Calamante, M.; Mordini, A.; Dessì, A. Dye-Sensitized Heterogeneous Photocatalysts for Green Redox Reactions. *Eur. J. Inorg. Chem.* **2020**, *2020*, 899−917.

(5) Yun, S.; Vlachopoulos, N.; Qurashi, A.; Ahmad, S.; Hagfeldt, A. Dye Sensitized Photoelectrolysis Cells. *Chem. Soc. Rev.* **2019**, *48*, 3705−3722.

(6) Vedhanarayanan, B.; Chen, C.-C.; Lin, T.-W. Plasmon-Enhanced Photocatalytic Hydrogen Production by Dual Dye Sensitized Ternary Composite of MoS3/ Au Core-Ag Shell Nanoparticles/ Graphene. *J. Power Sources* **2020**, *477*, 229033.

(7) Wang, D.; Li, Y.; Li Puma, G.; Wang, C.; Wang, P.; Zhang, W.; Wang, Q. Dye-Sensitized Photoelectrochemical Cell on Plasmonic Ag/AgCl @ Chiral TiO2 Nanofibers for Treatment of Urban Wastewater Effluents, with Simultaneous Production of Hydrogen and Electricity. *Appl. Catal., B* **2015**, *168−169*, 25−32.

(8) Zeng, J.; Zeng, W.; Zeng, H. In Situ Plasmonic Au Nanoparticle Anchored Nickel Ferrite: An Efficient Plasmonic Photocatalyst for Fluorescein-Sensitized Hydrogen Evolution under Visible Light Irradiation. *J. Solid State Chem.* **2017**, *253*, 294−304.

(9) Hou, W.; Pavaskar, P.; Liu, Z.; Theiss, J.; Aykol, M.; Cronin, S. B. Plasmon Resonant Enhancement of Dye Sensitized Solar Cells. *Energy Environ. Sci.* **2011**, *4*, 4650−4655.

(10) Chien, T.-m.; Pavaskar, P.; Hung, W. H.; Cronin, S.; Chiu, S.-H.; Lai, S.-N. Study of the Plasmon Energy Transfer Processes in Dye Sensitized Solar Cells. *J. Nanomater.* **2015**, *2015*, No. e139243.

(11) Ding, I.-K.; Zhu, J.; Cai, W.; Moon, S.-J.; Cai, N.; Wang, P.; Zakeeruddin, S. M.; Grätzel, M.; Brongersma, M. L.; Cui, Y.; McGehee, M. D. Plasmonic Dye-Sensitized Solar Cells. *Adv. Energy Mater.* **2011**, *1*, 52−57.

(12) Mandal, P.; Sharma, S. Progress in Plasmonic Solar Cell Efficiency Improvement: A Status Review. *Renew. Sustain. Energy Rev.* **2016**, *65*, 537−552.

(13) Rho, W.-Y.; Song, D. H.; Yang, H.-Y.; Kim, H.-S.; Son, B. S.; Suh, J. S.; Jun, B.-H. Recent Advances in Plasmonic Dye-Sensitized Solar Cells. *J. Solid State Chem.* **2018**, *258*, 271−282.

(14) Pandikumar, A.; Lim, S.-P.; Jayabal, S.; Huang, N. M.; Lim, H. N.; Ramaraj, R. Titania@gold Plasmonic Nanoarchitectures: An Ideal Photoanode for Dye-Sensitized Solar Cells. *Renew. Sustain. Energy Rev.* **2016**, *60*, 408−420.

(15) Rai, P. Plasmonic Noble Metal@metal Oxide Core−Shell Nanoparticles for Dye-Sensitized Solar Cell Applications. *Sustain. Energy Fuels* **2019**, *3*, 63−91.

(16) Ding, I.-K.; Zhu, J.; Cai, W.; Moon, S.-J.; Cai, N.; Wang, P.; Zakeeruddin, S. M.; Grätzel, M.; Brongersma, M. L.; Cui, Y.; McGehee, M. D. Plasmonic Back Reflectors: Plasmonic Dye-Sensitized Solar Cells. *Adv. Energy Mater.* **2011**, *1*, 51.
(17) Gong, J.; Liang, J.; Sumathy, K. Review on Dye-Sensitized Solar Cells (DSSCs): Fundamental Concepts and Novel Materials. *Renew. Sustain. Energy Rev.* **2012**, *16*, 5848−5860.
(18) Ramakrishnan, S. B.; Tirumala, R. T. A.; Mohammadparast, F.; Mou, T.; Le, T.; Wang, B.; Andiappan, M. Plasmonic photocatalysis. *Catalysis* **2021**, *33*, 38−86.
(19) Linic, S.; Christopher, P.; Ingram, D. B. Plasmonic-Metal Nanostructures for Efficient Conversion of Solar to Chemical Energy. *Nat. Mater.* **2011**, *10*, 911−921.
(20) Jain, P. K.; Lee, K. S.; El-Sayed, I. H.; El-Sayed, M. A. Calculated Absorption and Scattering Properties of Gold Nanoparticles of Different Size, Shape, and Composition: Applications in Biological Imaging and Biomedicine. *J. Phys. Chem. B* **2006**, *110*, 7238−7248.
(21) Li, J.; Cushing, S. K.; Meng, F.; Senty, T. R.; Bristow, A. D.; Wu, N. Plasmon-Induced Resonance Energy Transfer for Solar Energy Conversion. *Nat. Photonics* **2015**, *9*, 601−607.
(22) Cushing, S. K.; Li, J.; Bright, J.; Yost, B. T.; Zheng, P.; Bristow, A. D.; Wu, N. Controlling Plasmon-Induced Resonance Energy Transfer and Hot Electron Injection Processes in Metal@TiO2 Core−Shell Nanoparticles. *J. Phys. Chem. C* **2015**, *119*, 16239−16244.
(23) Hartland, G. V.; Schatz, G. Virtual Issue: Plasmon Resonances - A Physical Chemistry Perspective. *J. Phys. Chem. C* **2011**, *115*, 15121−15123.
(24) Mohammadparast, F.; Ramakrishnan, S. B.; Khatri, N.; Tirumala, R. T. A.; Tan, S.; Kalkan, A. K.; Andiappan, M. Cuprous Oxide Cubic Particles with Strong and Tunable Mie Resonances for Use as Nanoantennas. *ACS Appl. Nano Mater.* **2020**, *3*, 6806−6815.
(25) Chang, L.; Besteiro, L. V.; Sun, J.; Santiago, E. Y.; Gray, S. K.; Wang, Z.; Govorov, A. O. Electronic Structure of the Plasmons in Metal Nanocrystals: Fundamental Limitations for the Energy Efficiency of Hot Electron Generation. *ACS Energy Lett.* **2019**, *4*, 2552−2568.
(26) Tzarouchis, D.; Sihvola, A. Light Scattering by a Dielectric Sphere: Perspectives on the Mie Resonances. *Appl. Sci.* **2018**, *8*, 184.
(27) Kuznetsov, A. I.; Miroshnichenko, A. E.; Brongersma, M. L.; Kivshar, Y. S.; Luk'yanchuk, B. Optically Resonant Dielectric Nanostructures. *Science* **2016**, *354*, aag2472.
(28) Sugimoto, H.; Fujii, M. Colloidal Mie Resonators for All-Dielectric Metaoptics. *Adv. photonics* **2021**, *2*, 2000111.
(29) Cortés, E. Efficiency and Bond Selectivity in Plasmon-Induced Photochemistry. *Adv. Opt. Mater.* **2017**, *5*, 1700191.
(30) Caldarola, M.; Albella, P.; Cortés, E.; Rahmani, M.; Roschuk, T.; Grinblat, G.; Oulton, R. F.; Bragas, A. V.; Maier, S. A. Non-Plasmonic Nanoantennas for Surface Enhanced Spectroscopies with Ultra-Low Heat Conversion. *Nat. Commun.* **2015**, *6*, 7915.
(31) Poblet, M.; Li, Y.; Cortés, E.; Maier, S. A.; Grinblat, G.; Bragas, A. V. Direct Detection of Optical Forces of Magnetic Nature in Dielectric Nanoantennas. *Nano Lett.* **2020**, *20*, 7627−7634.
(32) Cambiasso, J.; König, M.; Cortés, E.; Schlücker, S.; Maier, S. A. Surface-Enhanced Spectroscopies of a Molecular Monolayer in an All-Dielectric Nanoantenna. *ACS Photonics* **2018**, *5*, 1546−1557.
(33) Addanki Tirumala, R. T.; P. Dadgar, A.; Mohammadparast, F.; Ramakrishnan, S. B.; Mou, T.; Wang, B.; Andiappan, M. Homogeneous versus Heterogeneous Catalysis in Cu 2 O-Nanoparticle-Catalyzed C−C Coupling Reactions. *Green Chem.* **2019**, *21*, 5284−5290.
(34) Pary, F. F.; Tirumala, R. T. A.; Andiappan, M.; Nelson, T. L. Copper(i) oxide nanoparticle-mediated C-C couplings for synthesis of polyphenylenediethynylenes: evidence for a homogeneous catalytic pathway. *Catal. Sci. Technol.* **2021**, *11*, 2414−2421.
(35) Rochkind, M.; Pasternak, S.; Paz, Y. Using Dyes for Evaluating Photocatalytic Properties: A Critical Review. *Molecules* **2014**, *20*, 88−110.
(36) Yan, X.; Ohno, T.; Nishijima, K.; Abe, R.; Ohtani, B. Is Methylene Blue an Appropriate Substrate for a Photocatalytic Activity Test? A Study with Visible-Light Responsive Titania. *Chem. Phys. Lett.* **2006**, *429*, 606−610.
(37) Marimuthu, A.; Zhang, J.; Linic, S. Tuning Selectivity in Propylene Epoxidation by Plasmon Mediated Photo-Switching of Cu Oxidation State. *Science* **2013**, *339*, 1590−1593.
(38) Oguike, R. S.; Kolo, A. M.; Shibdawa, A. M.; Gyenna, H. A. Density Functional Theory of Mild Steel Corrosion in Acidic Media Using Dyes as Inhibitor: Adsorption onto Fe(110) from Gas Phase. *ISRN Physical Chemistry* **2013**, *2013*, 1−9.
(39) Zheng, S.; Lu, J.; Shi, J.; Duan, X. Two-Dimensional Confined Electron Donor−Acceptor Co-Intercalated Inorganic/Organic Nanocomposites: An Effective Photocatalyst for Dye Degradation. *RSC Adv.* **2017**, *7*, 2789−2795.

https://doi.org/10.1021/acsanm.2c00730
ACS Appl. Nano Mater. 2022, 5, 6699−6707